ISSN: 2278-4632
Vol-10 Issue-1 January 2020

ENVIRONMENTAL FACTORS CLOSE TO THE SURFACE'S IMPACT ON THE INSTABILITY OF A SLOPE WITH UNSATURATED SOIL

[1*] *Deepali Barik,* [2]*Pankaj Joshi*
[1*] *Professor, Dept. of Civil Engineering, NIT BBSR,*
Asst. Professor Dept. of Civil Engineering, MITM, BBSR
[1*]*deepalibarik@thenalanda.com, joshipankaj@gmail.com*

Abstract: Two shallow slope failures appeared in the right-of-way of Provincial Road 259 in Virden, Manitoba, in 1999 following a period of heavy rain. Rainfall caused soil suction in the near-surface soil to dissipate, which decreased shear resistance and led to collapse. To determine the process of failure, a study effort was started by the Geotechnical Group at the University of Manitoba and the Manitoba Department of Highways and Transportation. To determine the reason for failure, the study involved a field investigation programme, laboratory testing programme, and sophisticated numerical modelling.

The findings show that the rains caused the suction in the soil slope to dissipate, which decreased the soil's shear strength and caused shallow collapses. A time-dependent seepage model that takes into account the flux boundary condition that occurred at the ground surface has been used to simulate the dissipation of the soil suction.

Key words: slope stability, unsaturated soils, laboratory tests, soil suction, seepage modeling, flux boundary.

Introduction

In geotechnical practise, the impact of suction on the stability of naturally occurring and artificially constructed slopes has grown in importance (Fredlund and Rahardjo 1993). A decrease of soil suction brought on by regional meteorological conditions has been linked to instability in specific case histories from Hong Kong, Singapore, Malaysia, and more recently Canada (Krahn et al. 1989; Brand et al. 1984; Lim et al. 1996).

Two bowl-shaped slope failures appeared in the right-of-way of Provincial Road 259 in 1999, 4 km northeast of Virden, Manitoba, following a period of intense rainfall (Fig. 1). The movements are located along a cut slope at the top of the Assiniboine River valley (Figs. 1, 2). Both slides occurred along a 200 m section of highway and showed similar failure geometry. In both cases, the head scarp initiated below the crest of the slope, and the surface of rupture exited above the slope toe. The slide masses were shallow, reaching a maximum depth of approximately 3.5 m at the midway point in the slide mass. This geometry is consistent with the slope failures noted in Krahn et al. (1989). Based on the long period of rainfall prior to the movements and the geometry of the failures, we postulate that infiltration associated with the rainfall caused dissipation of soil suction (negative pore-water pressures) in the soil profile, and that this, in turn, reduced the shear strength, thereby triggering failure. Since the slopes had been stable for approximately 30 years following construction, it seemed reasonable that the unusually long period of rainfall in 1999 was the triggering mechanism. The difficulty with verifying that suction dissipation triggered movements lies in assessing the in situ suction conditions at the time of failure and the time-dependent mechanism of rainfall infiltration.

The development of integrated software tools in which transient groundwater flow conditions can be imported into traditional limit equilibrium slope stability analyses allows evaluation of time-dependent pore-water pressure conditions

ISSN: 2278-4632
Vol-10 Issue-1 January 2020

Fig. 1. Aerial photograph of the study area taken in November 1999.

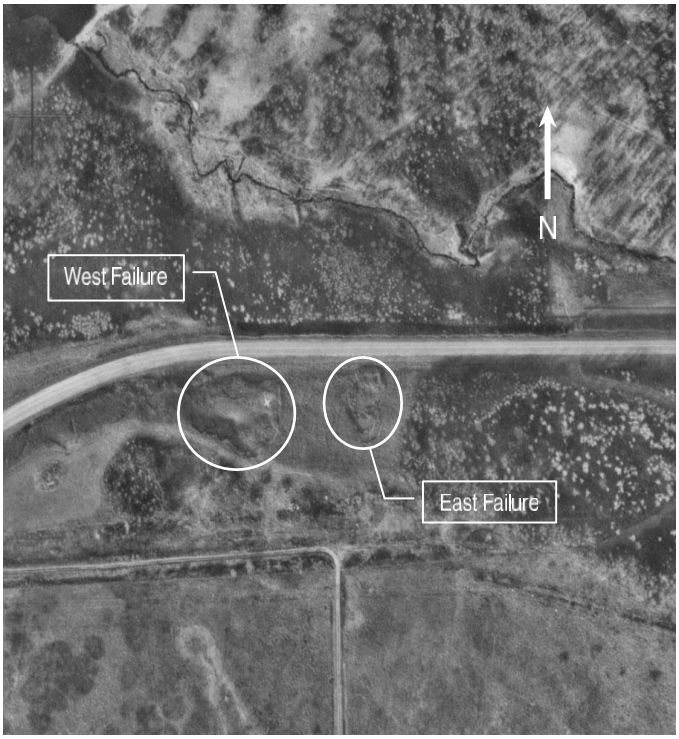

for many applications. For example, Misfeldt et al. (1991) modeled infiltration of water under flood conditions fol- lowed by subsequent rapid drawdown. The change in factor of safety for soil slopes following a short period of flooding could not be accurately predicted using simple traditional limit equilibrium approaches. A more detailed analysis that incorporates time-dependent infiltration into the slope during the flood stage needed to be included if the pore-water pres- sure response during subsequent drawdown to normal river conditions was to be accurately predicted. Similarly, Tutkaluk et al. (1998) examined the effect of high piezometric levels in a confined aquifer on slope stability of lacustrine clay riverbanks along the Red River in the City of Winnipeg. Connection between pore-water pressures in the clay and the upper carbonate aquifer was clearly recorded with monitoring wells in many parts of the city. The aquifer was affected by regional recharge from a number of loca- tions, by pumping in the summer for cooling processes, and by regulated river levels at the toe of the slope in the fall. The coupling of pore-water pressures with the transient piezometric conditions in the upper carbonate aquifer was assessed using a time-dependent groundwater model. Under- standing transient groundwater potentials provided an under-

standing as to why it has previously been difficult to predict riverbank failure along the Red River (Baracos and Graham 1981). This paper uses a similar transient modeling approach to examine how infiltration due to rainfall over a long period affects pore-water pressures and therefore the factor of safety in soil slopes.

The objective of the research was to develop a numerical model to examine the influence of transient infiltration con- ditions associated with rainfall events to obtain a better un- derstanding of why the Provincial Road 259 slopes failed after 30 years of being stable.

General overview of the site

ISSN: 2278-4632
Vol-10 Issue-1 January 2020

Both the East and West failures (Fig. 1) occurred in the spring of 1999 on a 3.4H:1V (~17° from horizontal) north- facing cut slope. The failures had shallow, bowl-shaped ge- ometries, ranging in depth from 2.0 to 3.5 m. The head scarps initiated at or below the crest, and the surfaces of rup- ture exited above the slope toe. The geometry of the failures suggested combined sliding and rotational movements. Be-
tween the summers of 1999 and 2000, the two failures were repaired by Manitoba Department of Highways and Trans-

.

Fig. 2. Topographic map and photographs of the study area. Contours in metres. PR259, Provincial Road 259.

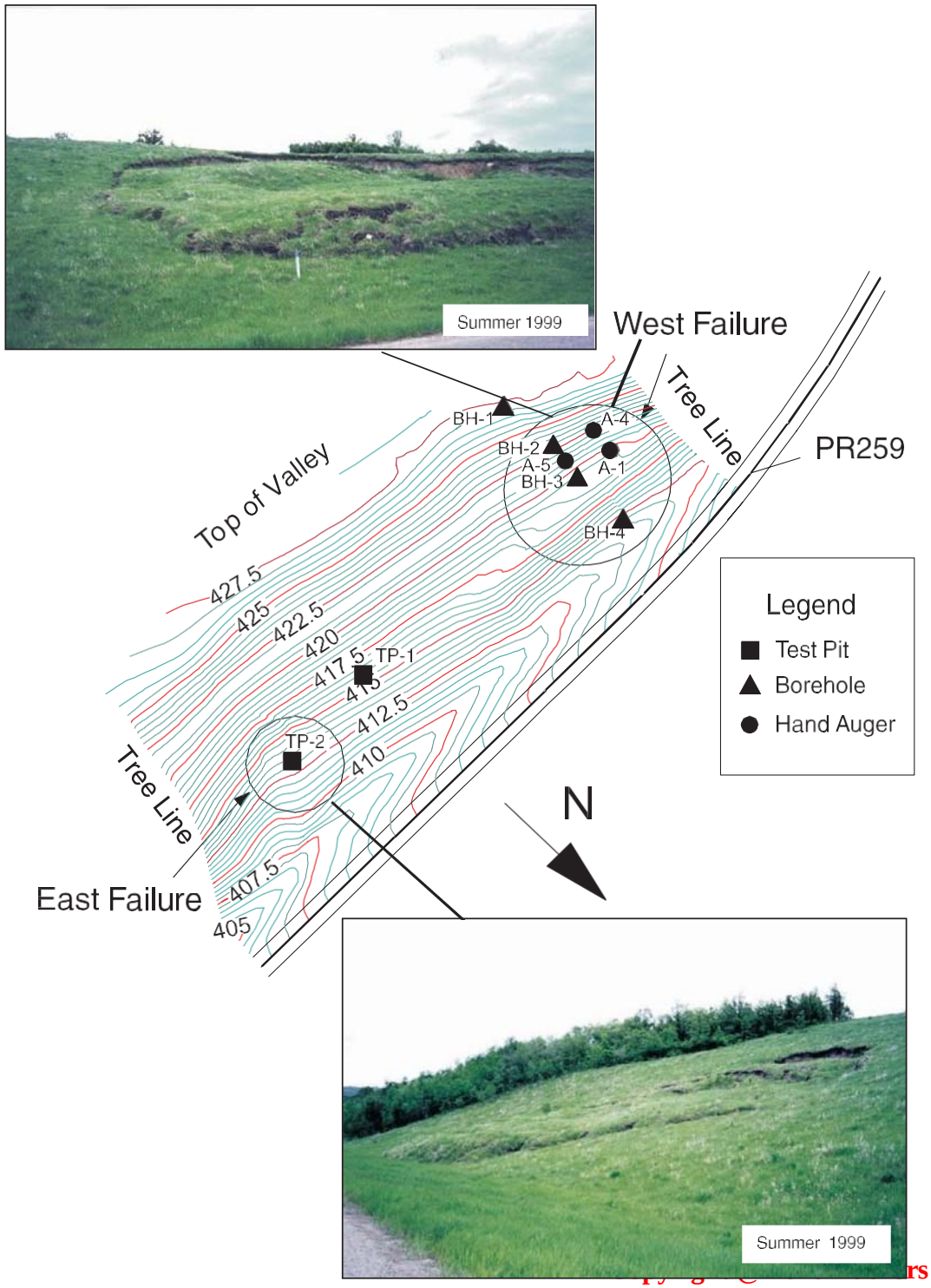

ISSN: 2278-4632
Vol-10 Issue-1 January 2020

portation. The West failure (Fig. 2) was benched approxi- mately midway up the slope, and the East failure was simply reworked back to original grade with no stabilization mea- sures.

Following these repairs, both failures moved again in the summer of 2001. The new movement of the East failure was approximately half the size of the original mass and approxi- mately the same depth. The West failure moved once more following rainfall in early July 2001. From aerial photo- graphs taken after the initial slope failures, the reactivated West failure appears to be approximately the same size asthe original slope failure.

The soil along the slope face is a clayey silt loam with some weathered clay shale and other gravel-sized debris in- cluding rock fragments of igneous and metamorphic origin. The presence of sedimentary, igneous, and metamorphic li-

Fig. 3. Bedrock geology of the study area (Betcher 1983). R, range; T, township.

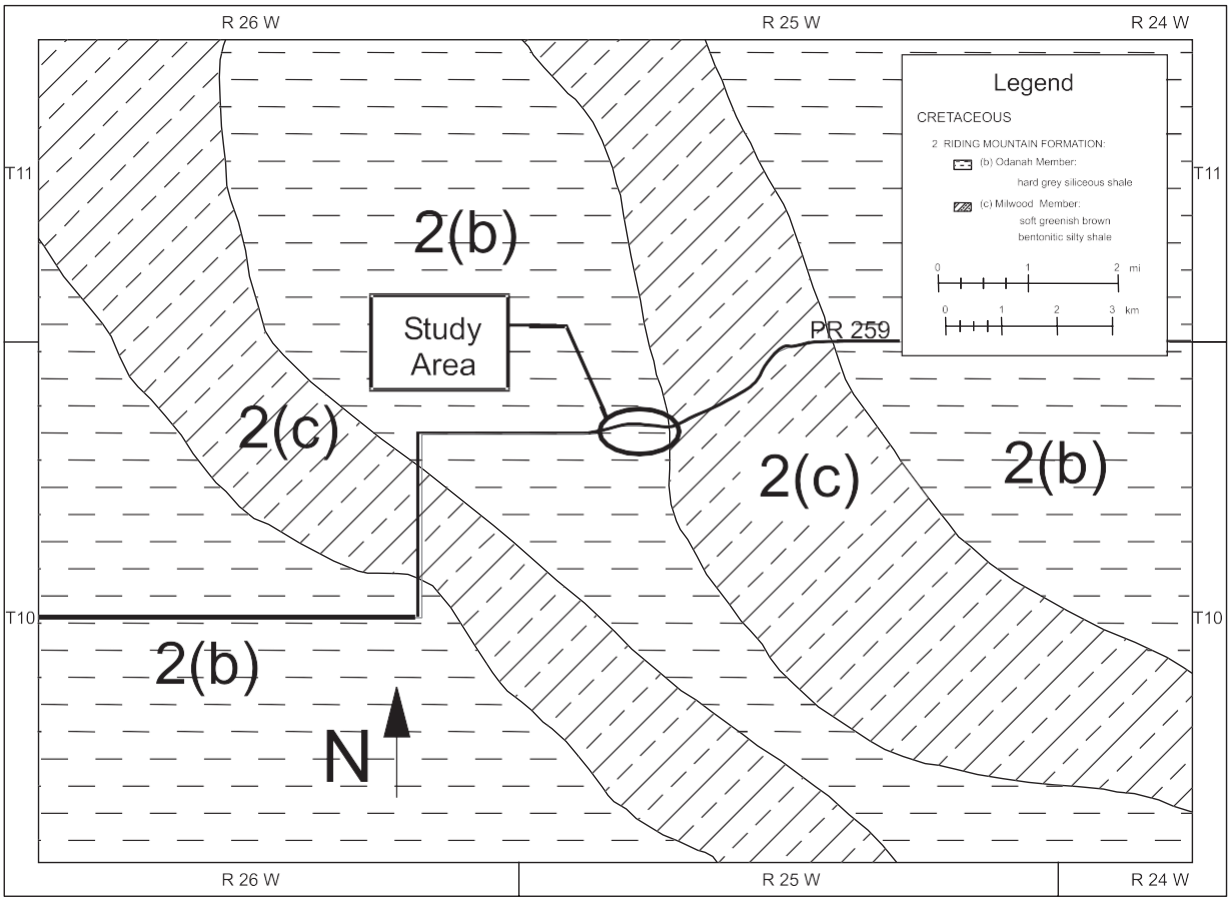

thology is evidence of past glacial activity. At and beyond the slope crest, the surficial deposits consist typically of till that includes clay- to boulder-sized material.

Site geology and geomorphology

The stratigraphy at the location of the failures encom- passes a complex geological profile produced by several geomorphological processes. The study area is located within the Souris Basin physiographic division near the edge of the Assiniboine River valley. The local overburden mate- rial includes water-laid till, alluvium, lacustrine clays, and silts all deposited about 12 000 – 14 000 years before pres-ent (Klassen and Wyder 1970; Klassen 1975).

ISSN: 2278-4632
Vol-10 Issue-1 January 2020

The Assiniboine River valley system in general is of gla- cial origin, evidenced by the shape and position of valleys that are parallel to the regional slope and ride over the topo- graphic highs. The valley, for the most part, was formed be- fore the last glaciation, during the Early Wisconsinan. There are several locations along the river, including the study area, where the present Assiniboine valley breaks away from the ancestral valley referred to as the Virden valley. The two valleys can be clearly interpreted from the bedrock geology (Fig. 3). The study area is located over hard gray siliceous shale known as the Odanah Member between the ancestral Virden valley that lies to the west and the Assiniboine valley to the east. Both valleys are underlain by the Milwood Mem- ber composed of soft green bentonitic silty shale (Betcher 1983). The shale outcrops to the east of the Assiniboine val-

ley and has produced another landslide (on the opposite side of the river valley) with quite different morphology and a deep-seated failure mechanism that is controlled by the ori- entation and properties of the bentonitic shale.

Surficial deposits along the Assiniboine River valley include till, glaciolacustrine clay, silt, alluvium, sand and gravel, and occasional bedrock outcrops. Figure 4 shows a map of surficial deposits in the region (Betcher 1983). The study area is in a transition zone consisting of till and allu- vium deposits that give a highly variable stratigraphic pro- file. The shallow nature of the slide movements suggests that geological complexity does not play a major role in the de- velopment of the failures.

Field investigation

Our preliminary site visit obtained grab samples for clas- sification and installed shallow standpipes in the West failure. Results of the classification tests and standpipe mea- surements from the field were used to develop a more- detailed field investigation program that included two testpits and four boreholes with piezometer installations.

Test pits

Two test pits were excavated in the cut slope. Test pit 1 (TP-1) was excavated just west of the East failure in intact (stable) material, and test pit 2 (TP-2) was excavated in the East failure slide mass (Fig. 2).

.**Fig. 4.** Surficial deposits of the study area (Betcher 1983).

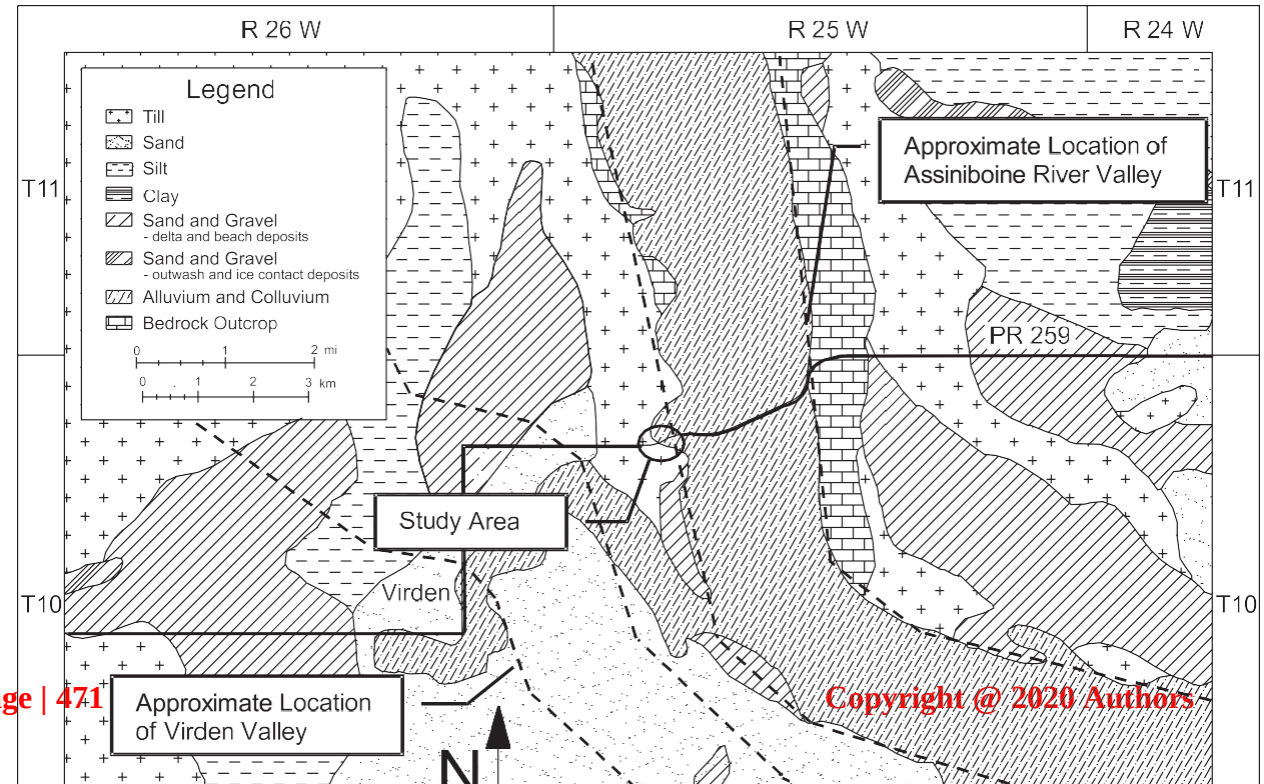

ISSN: 2278-4632
Vol-10 Issue-1 January 2020

Test pit 1 was excavated to 5 m depth. The profile com- prised silty clay material of low to medium plasticity with a blocky and friable structure. A possible failure surface was identified at a depth of approximately 2.7 m. The failure sur- face was noted as having a slickensided appearance, indicat- ing large movements at that depth. The slickensided surface dipped at approximately 15° from the horizontal, which roughly matched the inclination of the ground surface (~17°). Below 3.4 m, the silty clay showed evidence of past move- ments in the form of slickensided surfaces and a soft dis- turbed zone. Since test pit 1 was outside the zone of failed material, the presence of the slickensided surfaces suggested the existence of past movements, although none were notedin historic records.

In test pit 1, block samples were taken at depths of 1.5and 2.5 m for laboratory testing. Block samplers developed at the University of Manitoba that allow for retrieval of large volumes of intact material (44 cm × 22 cm × 22 cm) were used to ensure minimal disturbance of the extracted materi- als (Domaschuk 1977).

Test pit 2 showed a similar soil profile, although with greater variability near the surface. This variability was likely caused by slope regrading undertaken following the initial failure in 1999. Test pit 2 was excavated to a depth of
3.8 m. A slickensided surface was visible on the walls and bottom of the pit at a depth of 2.9 m (Fig. 5). This slicken- sided surface was identified as the rupture surface of the

1999 failure. It dipped at approximately 22° from the hori- zontal, which is again broadly similar to the inclination ofthe slope face (~17°).

A Quickdraw tensiometer (Soilmoisture Equipment Corp., Santa Barbara, Calif.) was used to measure the matric suc- tion profile in the side walls of the test pits at intervals of
0.5 m below ground surface until a zero suction reading was obtained. The tensiometer is well known in soil science and is not described further (see, for example, Krahn et al. 1989). Figure 6 shows the variation of tensiometer readings (matric suction) with depth in the test pits. Suctions de- creased from about 75 kPa at 0.5–1.0 m depth to 0 kPa at 2.0–2.5 m depth. A distinct shift in the soil suction profile was noted in both pits at a depth of 1.0–1.5 m, indicating an existing gradient likely due to recent weather conditions.

Boreholes and standpipe installation

The first borehole (BH-1) was drilled at the crest of the slope to a depth of 24.4 m (Fig. 2). The other three bore- holes (BH-2, BH-3, BH-4) were drilled to 5.2–7.2 m depthin the regraded West failure. Standpipes with Casagrande tips were installed in all holes to obtain a record of ground- water changes from that time forward. Sand was placed atthe location of the tip and presaturated during installation. The remaining length of the installation was backfilled witha bentonite seal to isolate the sand-packed section and then**Fig. 5.** Failure surface at the bottom of test pit 2. The spatula is approximately 30 cm long.

Fig. 6. Suction profiles measured in test pits. GSE, ground sur-face elevation.

ISSN: 2278-4632
Vol-10 Issue-1 January 2020

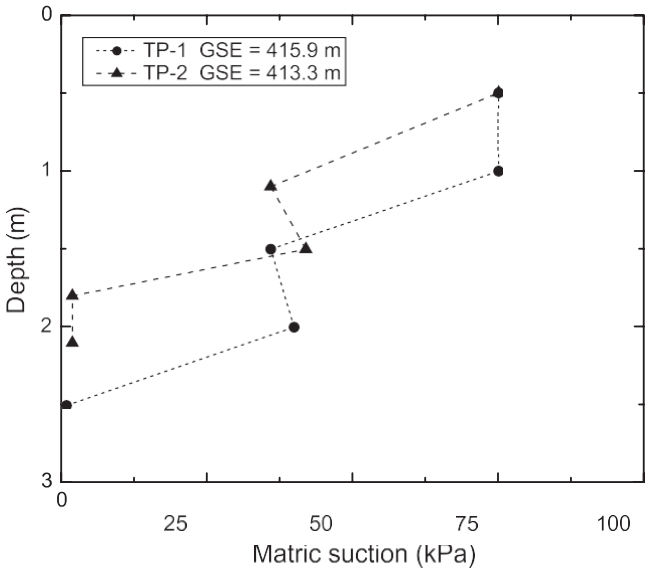

clay cuttings to ensure the measured pressure reflected the conditions at the elevation of the tip.

The borehole log for BH-1 (Fig. 7) indicates the typical profile at the site. Numerous fractures were recorded in BH-1, BH-2, and BH-3. For the most part these fractures were oriented roughly parallel to the inclination of the slope. The fractures were either infilled with a gray silty fine sand or were slickensided in nature. The failure surface for the West failure was interpreted from observations in the test pit.

Plotting the borehole and hand auger information demon- strated that the soil profile was highly variable. Groundwater

measurements were also variable, with only some standpipes (including borehole and hand-augured installations) showing evidence of water in the slope during typical operating con- ditions. The site variability confirms the complex nature of the deposits and the geomorphological processes that formed the area (Fig. 4). Four simplified layers were interpreted from the observed soil profile to use on the numerical mod- eling (Fig. 8). From the surface downwards, these include
(*i*) a near-surface silty clay layer with a weathered zone (evi- dent by a blocky–friable structure that suggests a weathered zone produced by environmental conditions); (*ii*) a silty fine sand seam below the clay, extending from behind the crest to approximately mid-slope; (*iii*) an unweathered clayey silt layer beneath the weathered zone and the silty fine sand seam; and (*iv*) a silt – fine sand layer beneath the clay layer at a considerable depth relative to the slope failures. The simplified layers are indicated on the right-hand side of the borehole log (BH-1) in Fig. 7. The simplified units have been interpreted from the multiple boreholes, and average positions of the stratigraphic interfaces have been assumed. As such, the simplified layers do not exactly conform with the BH-1 log in Fig. 7. Giving consideration to length con- straints, detailed descriptions of the borehole logs and the simplifications used for modeling have not been included here. Detailed records of the site investigation are available in Ferreira (2002).

Laboratory testing

Laboratory testing consisted of traditional soil classifica- tion tests, flexible-wall permeameter tests, triaxial tests, and direct shear tests to determine soil properties necessary for detailed modeling.

ISSN: 2278-4632
Vol-10 Issue-1 January 2020

Fig. 7. Borehole log for BH-1 (GSE = 427.14 m). EOH, end of hole; I_P , plasticity index; w_L, liquid limit; w_n, natural water content; w_P , plastic limit.

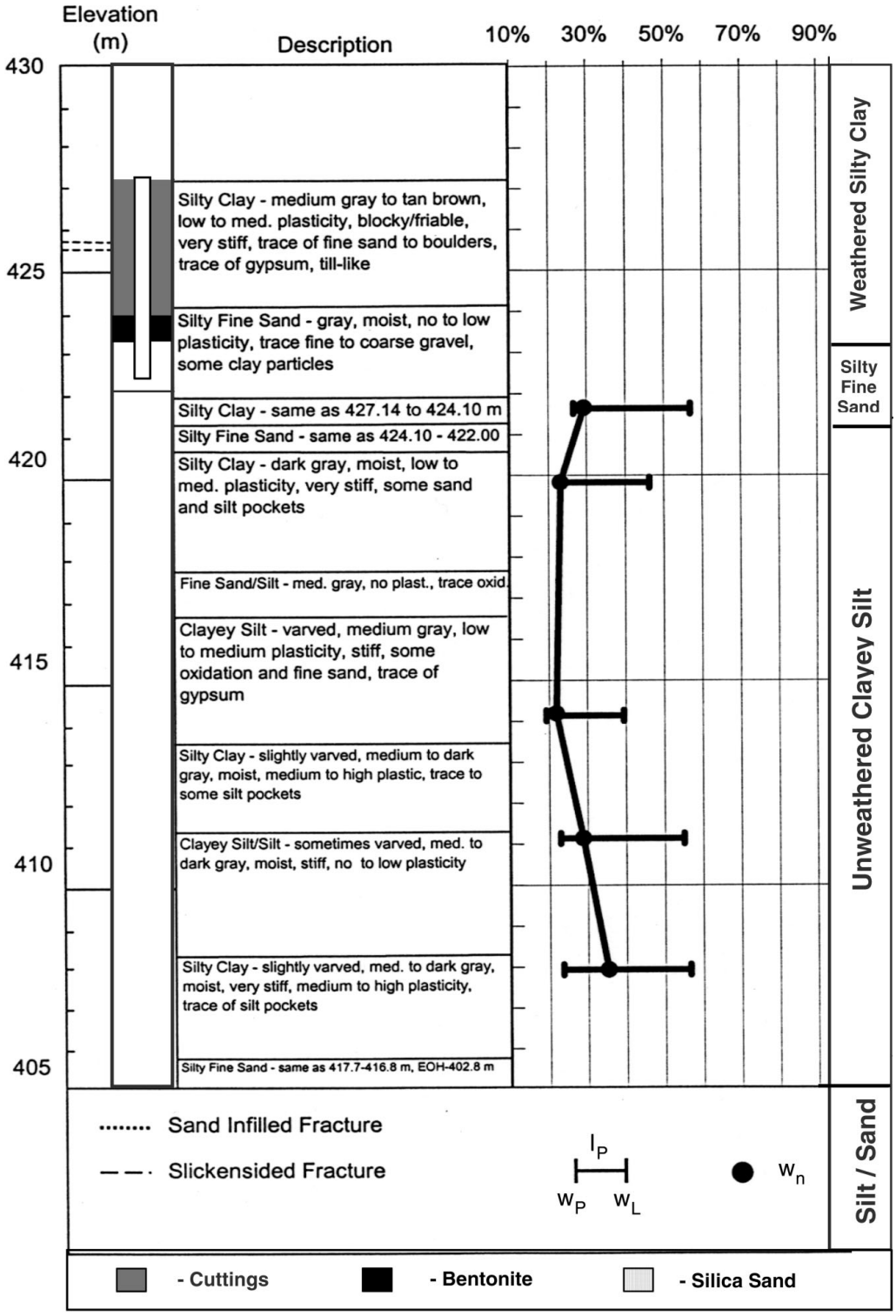

ISSN: 2278-4632
Vol-10 Issue-1 January 2020

Fig. 8. Model stratigraphy used for numerical analysis. CL, centreline of road PR259.

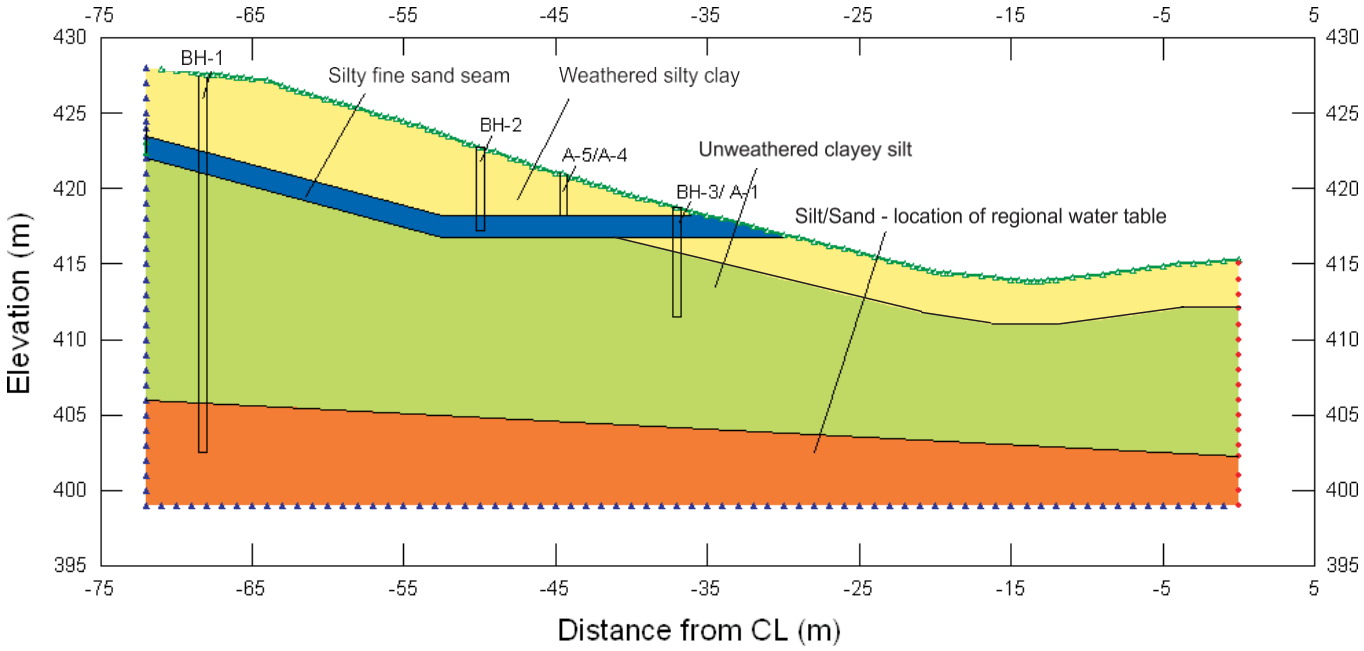

Soil classification

In total, 30 classification tests were performed on material retrieved from the study area. Tests included Atterberg lim- its, specific gravityhydrometer, and sieve analysis. Water contents were measured on all samples.

Figure 7 shows water content and Atterberg limits versus elevation for BH-1. Plastic limits ranged typically from 18% to 20%, and liquid limits typically from 50% to 60%. The results of the plasticity index ranged from 30% to 40%. The in situ water contents were generally near or at the plastic limit corresponding to stiff material.

Flexible-wall permeameter tests

The hydraulic conductivity of the lower unweathered clay material was measured using six flexible-wall permeameter tests (in general accordance with the American Society for Testing and Materials (ASTM 1990) standard test methodD5084-90). Tests on samples taken from shallow depths of 1.7–4.4 m produced conductivity values ranging from 5.6×10^{-10} to 3.7×10^{-11} m/s. The confining pressure for all hy- draulic conductivity tests was 30 kPa to approximately repli- cate the in situ stress level. The blocky–friable nature of the weathered clay layer did not allow for laboratory testing. This was considered a weakness in the testing program, since it was clear that the fabric of the material would influ- ence its in situ bulk permeability. This means that the mea- sured values of hydraulic conductivity were most likely lower than the in situ values for the weathered silty clay. This point is addressed further in the modeling section when discussing how hydraulic conductivities were selected for seepage modeling.

Triaxial tests and direct shear tests

In total, seven isotropically consolidated undrained tri- axial compression tests with pore-water

ISSN: 2278-4632
Vol-10 Issue-1 January 2020

pressure measure-

ment (CIU tests) and six direct shear tests were performedon specimens from BH-2 and BH-3. Testing procedures for the CIU triaxial tests were in gen- eral accordance with ASTM standard test method D4767 (ASTM 1995). Due to the shallow nature of the slides, rela- tively low effective stresses of 70, 130, 150, and 190 kPa were selected for testing. The specimens were 71.1 mm in diameter, corresponding to the diameter of the Shelby tubes. Due to the stiffness and coarse fraction in most of the sam- ples, trimming to a smaller diameter for testing was avoided. The heights of the specimens ranged from 108 to 128 mm.

Figure 9*a* shows the triaxial stress paths in deviator stress versus mean effective stress space. Results for the inter- preted "post-peak" strengths of the CIU specimens produced a linear best-fit line with effective angle of shearing resis- tance for a normally consolidated soil, $\phi_n\phi_c$, equal to 22.3°, assuming the effective cohesion of normally consolidated soil $c_n\phi_c$ ≈ 0 (Fig. 9*b*). The parameter $\phi_n\phi_c$ was chosen as the most appropriate for the stability analysis due to the blocky structure of the material. Rivard and Lu (1978) demonstrated that $\phi_n\phi_c$ (and not $\phi_o\phi_c$, the effective angle of shearing resis- tance for an overconsolidated soil) appropriately defines the shear strength in similar materials. An average value of $\phi_n\phi_c$ was selected because the material itself is highly hetero-geneous and failures can be expected to develop when "aver- aged" shearing resistance has been generated. Consistent with Rivard and Lu, the cohesion for the material with nor- mally consolidated strengths was taken as zero.

Six direct shear tests were performed on specimens trimmed from samples extracted from Shelby tubes from boreholes BH-2 and BH-3. The direct shear testing proce- dures were in general accordance with ASTM standard test method D3080 (ASTM 1993). The samples were tested at vertical stresses that partially overlapped the lower range of confining pressures used in the triaxial tests. This was doneto more thoroughly understand the strength parameters for

Fig. 9. (*a*) Triaxial stress paths. (*b*) Triaxial testing summary ofpost-peak strengths. *M*, slope of post-peak strength envelope in *q*, *p*′-space. (*c*) Direct shear testing summary of post-peak strengths.

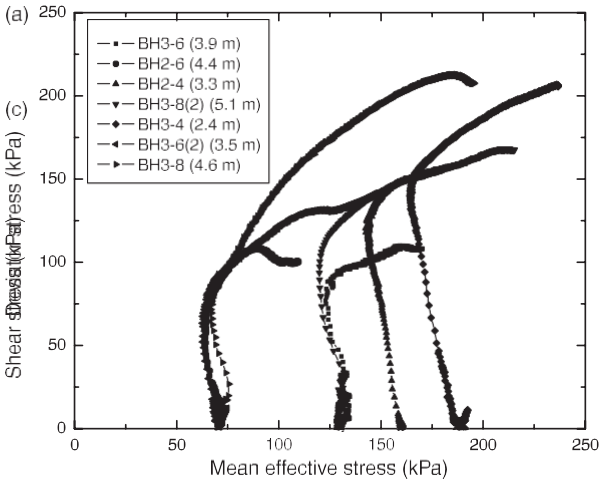

ISSN: 2278-4632
Vol-10 Issue-1 January 2020

Mean effective stress (kPa)
Normal stress (kPa)

the clayey silt. The vertical stresses used in the direct shear tests are 30, 60, and 90 kPa. The specimens were trimmed to
70.9 mm in diameter, which is 0.2 mm smaller than the di- ameter of the Shelby tubes. The average height of the direct shear specimens was 28.3 mm. Values of post-peak strengths from the direct shear tests produced a best-fit line with a friction angle $\phi_n\phi_c$ of 20.9° (Fig. 9*c*).

Modeling of saturated–unsaturated seepage and slope stability

Combined seepage and limit equilibrium slope stability analyses were used to model the failures using the soil prop- erties from the field and laboratory testing programs. The modeling was done using Seep/W and Slope/W (proprietary software products of Geo-Slope International, Ltd., Calgary, Alta.).

Transient seepage model

A transient model was constructed to show that the postu- lated mechanism of soil suction dissipation could be repro- duced in a numerical framework based on measurements from the site. The modeling covered a period of over200 days in each of two separate years. The first model was for the year 2000 when information on groundwater levels was available from standpipes installed during the site inves- tigation in the previous year. The soil suction profiles mea- sured in the test pits were used for calibrating the suction profiles in the numerical model.
Once the model input parameters were calibrated using measurements from the site, the model was reanalyzed using rainfall data from the 1999 database to assess whether the slope failures could be reproduced in the model.

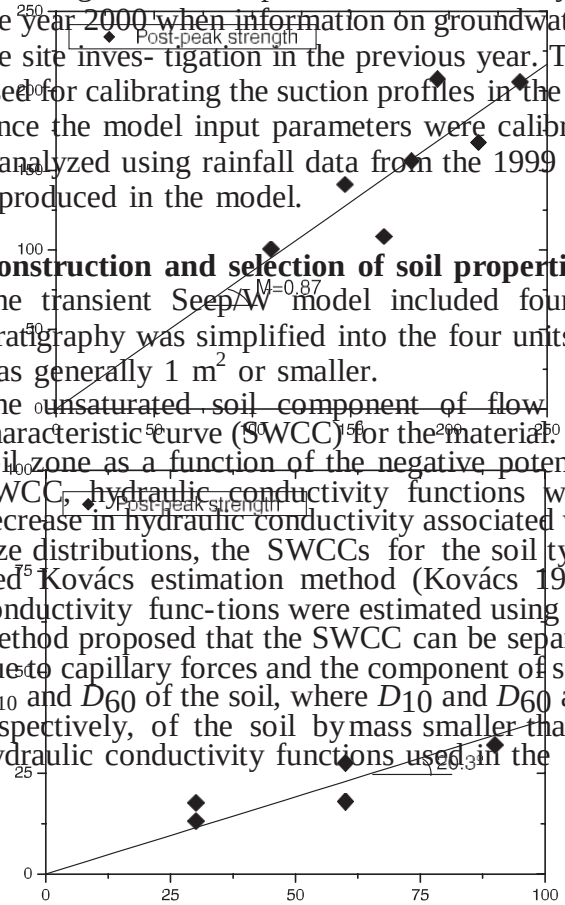

Construction and selection of soil properties

The transient Seep/W model included four soil layers in- terpreted from the field logs. The stratigraphy was simplified into the four units described previously (Fig. 8). The mesh element size was generally 1 m^2 or smaller.
The unsaturated soil component of flow in the upper weathered zone required a soil-water characteristic curve (SWCC) for the material. The SWCC incorporates the stor- age in the unsaturated soil zone as a function of the negative potentials that exist at any point in time. In addition to the SWCC, hydraulic conductivity functions were required for all materials to adequately model the decrease in hydraulic conductivity associated with decreases in suction. Based on the measured grain-size distributions, the SWCCs for the soil types in the study area were determined using the modi- fied Kovács estimation method (Kovács 1981; Aubertin et al. 1998), and the associated hydraulic conductivity func-tions were estimated using the van Genuchten method (1980). The Kovács (1981) method proposed that the SWCC can be separated into two components, the component of saturation due to capillary forces and the component of satu- ration due to adhesive forces. Both are based on the D_{10} and D_{60} of the soil, where D_{10} and D_{60} are the nominal particle diameters with 10% and 60%, respectively, of the soil by mass smaller than these diameters. Figure 10 shows typical SWCC and hydraulic conductivity functions used in the

ISSN: 2278-4632
Vol-10 Issue-1 January 2020

Fig. 10. Soil-water characteristic curves (SWCCs) and hydraulicconductivity functions for silty clay layer. □, volumetric water content; *k*, hydraulic conductivity; □, suction.

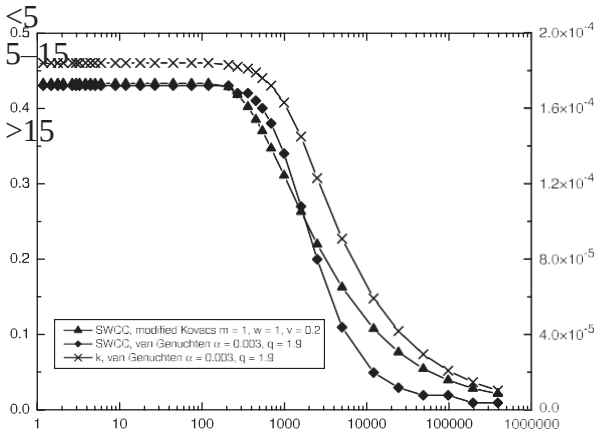

Table 1. Runoff coefficients.

Return period, T_R (years)	Runoff coefficient
<5	0.97
5–15	0.98
>15	0.99

ISSN: 2278-4632
Vol-10 Issue-1 January 2020

θ

k (m / day)

Ψ (kPa)

model. The SWCC generated represents the drying curve for the soil.

To provide better representation of the fissured materials seen in the field, the calculated SWCC and hydraulic con- ductivity function were adjusted to account for the presence of secondary structures caused by weathering affects. The saturated conductivity of the weathered clay used in the tran- sient Seep/W model (2.1×10^{-9} m/s) was taken as 10 times larger than the average saturated hydraulic conductivity mea- sured in the laboratory. This adjustment was made according to observations of the decrease in hydraulic conductivity for similar fissured materials in comparison with intact mea- sured values made by Shaw and Hendry (1998) and Viklander (1998).

The SWCC for the silt–sand seam was selected from curves provided by Geo-Slope International, Ltd., based on the measured grain-size distribution of the material. This was considered reasonable, since the silty fine sand seam was assumed to remain saturated and therefore would not use the nonlinear portion of the SWCC function (in the neg- ative pore-water pressure range). An average saturated hy- draulic conductivity of 5.7×10^{-2} m/day (6.6×10^{-7} m/s) determined from field slug tests was used for the modeling. The hydraulic conductivity used for the lower unweathered clay layer was taken as the average measured value from six flexible-walled permeameter tests without further adjust- ments, namely 1.8×10^{-5} m/day (2.1×10^{-10} m/s).

Boundary conditions

The selected boundary conditions for the section shown in Fig. 8 included a "no-flow" boundary along the bottom of the domain, indicating that flow through the cross section at the base was assumed to be horizontal. The left boundary for the unweathered and weathered clay layers was assigned as a no-flow condition, since the lateral flow in the low- permeability layers would be negligible compared with the flow resulting from the higher permeability of the silty fine sand seam. Based on measurements from the standpipes, a positive flux boundary condition was assigned to the silty fine sand seam at the left boundary to act as a groundwater recharge. The magnitude of the recharge was determinedduring calibration to ensure a match with observations from the standpipes. The right boundary of the domain incorpo- rated a constant head value of 402.1 m based on observed water levels from an unpublished consulting report for de- velopment at a nearby site.

An environmental flux boundary adjusted for potential seepage exiting on the ground surface was assigned to the slope face. This boundary condition incorporates a numberof environmental factors that occur at the near-surface envi- ronment. The environmental flux boundary function includes both evapotranspiration during periods with no rainfall and infiltration during rainfall events. The flux function was determined from relevant rainfall and temperature data ob- tained from an Environment Canada weather station near Virden, Manitoba. Infiltration during rainfall events incorpo- rated precipitation, evapotranspiration, and runoff based on the return period of the event. The infiltration was calculated based on the relationship

$$[1] \quad I = P - E - aP$$

where I is the infiltration (cm/day), P is the precipitation (cm/day), E is the evapotranspiration calculated using Meyer (1944) (cm/day), and a is a runoff coefficient based on the return period T_R.

The following paragraphs describe how the terms in eq. [1] were evaluated. Many factors affect the magnitude of evapotranspiration E in eq. [1]. Penman (1948) stated that the rate of evapotranspiration from sparsely vegetated and bare soil is approximately equal to the rate of evaporation from a free water surface provided that the supply and avail- ability of water to the surface are unlimited. A simple mass transfer equation for a free water

ISSN: 2278-4632
Vol-10 Issue-1 January 2020

surface presented by Meyer (1944) was used to determine the evapotranspiration, which would be used as a starting point prior to calibration. Meyer proposed an empirical mass transfer equation for Minnesota lakes:

[2] $E = 0.0106(1 + 0.1u)(e_S - e_a)2.54$

where E is evaporation from the free water surface (cm/day), u is the wind speed (mph), e_S is the saturated water vapour pressure (mbar), and e_a is the actual water vapour pressure (mbar).

It is recognized that this approach likely overestimates the amount of evapotranspiration. This is discussed further in a later section. For calculating runoff in eq. [1], three runoff coefficients were assigned to three ranges of return periods. The return periods were calculated using the last 40 years of rainfall data gathered from the Virden weather station. The first coefficient was assigned to rainfall events with less than a 5 year return period. The second runoff coefficient calcu- lated runoff for rainfall events with return periods between 5 and 15 years. The last runoff coefficient was assigned tolarge rainfall events having return periods greater than

.ig. 11. Calibrated environmental flux boundary function.**Fig. 12.** Modeled versus measured groundwater level

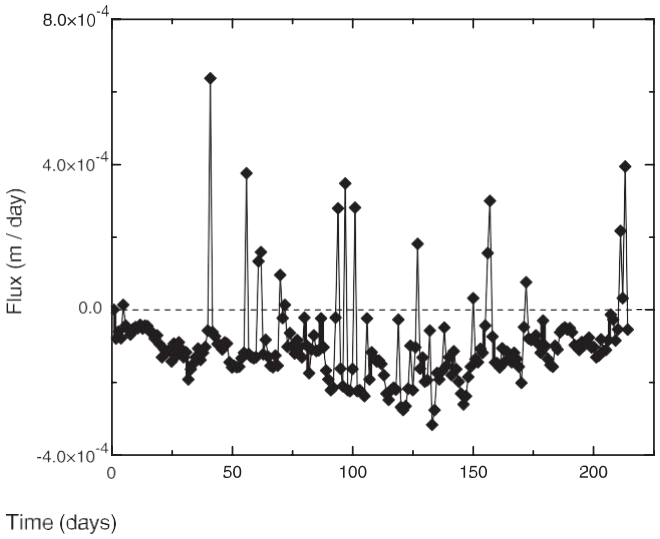

15 years. The runoff coefficients were adjusted during the calibration phase of the modeling to reach a reasonable match with the measured data. Table 1 shows runoff coeffi- cients used in the calibrated flux function.

The infiltration value (I in eq. [1]) represents a "potential" value as opposed to the actual value. This is due to the assumed inputs of potential evaporation and evapo- transpiration.

Limited environmental information available at this site did not allow use of more sophisticated flux boundary mod- els such as those developed by Wilson et al. (1994, 1997). Our approach was deemed appropriate, as the flux boundary function was adjusted during calibration of the model using measurements from the site. This moved the function closerto the actual infiltration. Further work is being done to eval- uate the flux boundary function using the more advanced methods proposed by Wilson et al.

Figure 11 shows the calibrated environmental flux bound- ary function that was used in the seepage model for year 2000. For the most part, the slope face was subjected to a negative flux or drying. There were several occasions, how- ever, where rainfall events were large enough to create a positive flux; that is, infiltration into the slope. The key question about the effect infiltration has on slope

ISSN: 2278-4632
Vol-10 Issue-1 January 2020

stability is whether it occurs for only a relatively short period of time or over an extended period.

Calibration of the seepage model

Calibrating the transient seepage model consisted of ad- justing the amount of recharge into the silty fine sand seam and at the same time adjusting the environmental flux func- tion to produce good agreement with measured in situ groundwater and soil suction profiles. Calibration was done for the period 1 April to November 2000 when groundwater levels and the soil suction profile were measured. After cali- bration, the recharge from the silty sand seam was reduced to achieve acceptable calibration with observed groundwater and suction measurements.

As expected, the calculated groundwater profile was found to be sensitive to rainfall events. To reduce thi effectin the upper weathered soil, the SWCC was adjusted relative

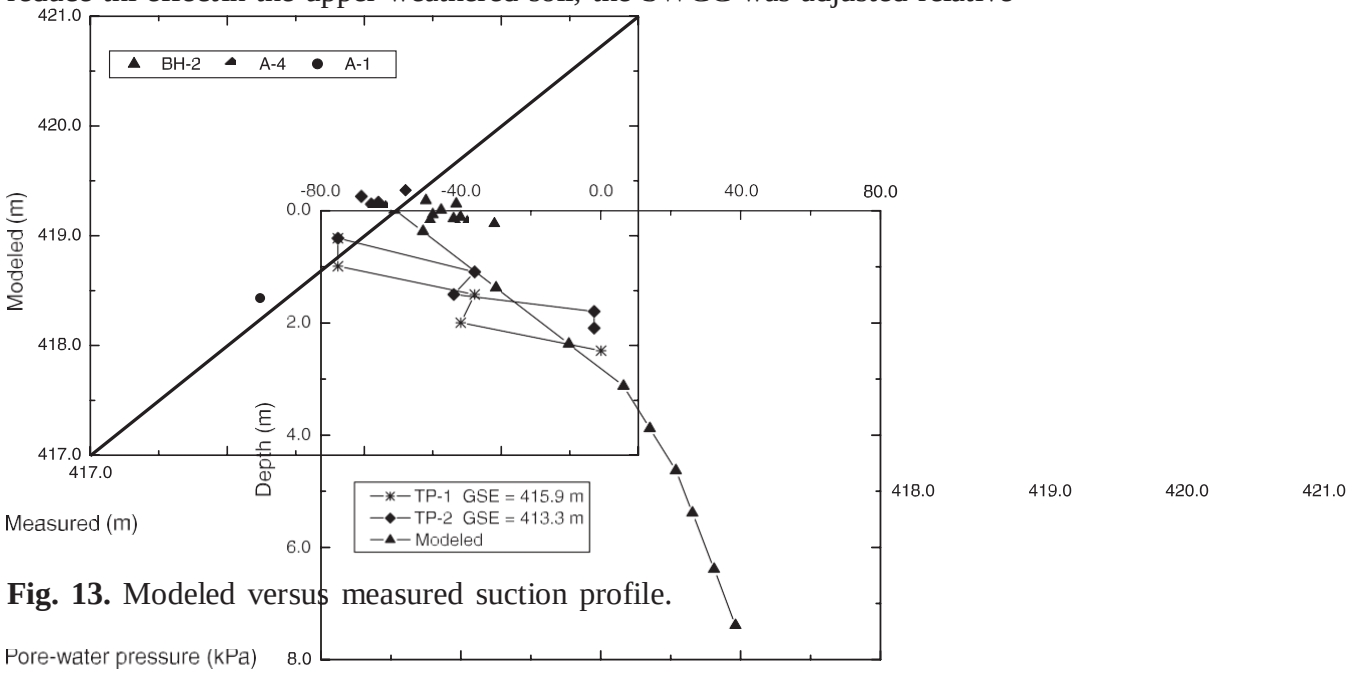

Fig. 13. Modeled versus measured suction profile.

to the air-entry value (AEV) to take into account its secondary structure. This modeled desaturation of the upper weathered silty clay at lower suctions. This adjustment was reasonable, as the fabric of the fissured weathered clay would also provide for storage additional to the capacity ofthe intact blocks. Adjusting the SWCC for the weathered soil in this way reduced the sensitivity of the groundwater profile to intense rainfall events. Since the AEV and the hy- draulic conductivity are related through the SWCC, the hy- draulic conductivity function was also adjusted.

Figures 12 and 13 show results of the calibration exercise. The modeled total heads (Fig. 12) show reasonable agree- ment with measured water levels. Similarly, the modeled suction profile compared reasonably well with the measured suction profiles from test pits TP-1 and TP-2 (Fig. 13). The modeled suction profile was not as steep as the measured profile in the unsaturated soil zone and displayed the ex-pected nonlinearity when the pore-water pressure went from negative to positive.

ISSN: 2278-4632
Vol-10 Issue-1 January 2020

Fig. 14. (*a*) Total head and environmental flux versus time.
(b) Suction and environmental flux versus time. The asterisks in the inset profiles show the location of the node near the ground surface at the toe of the slope.

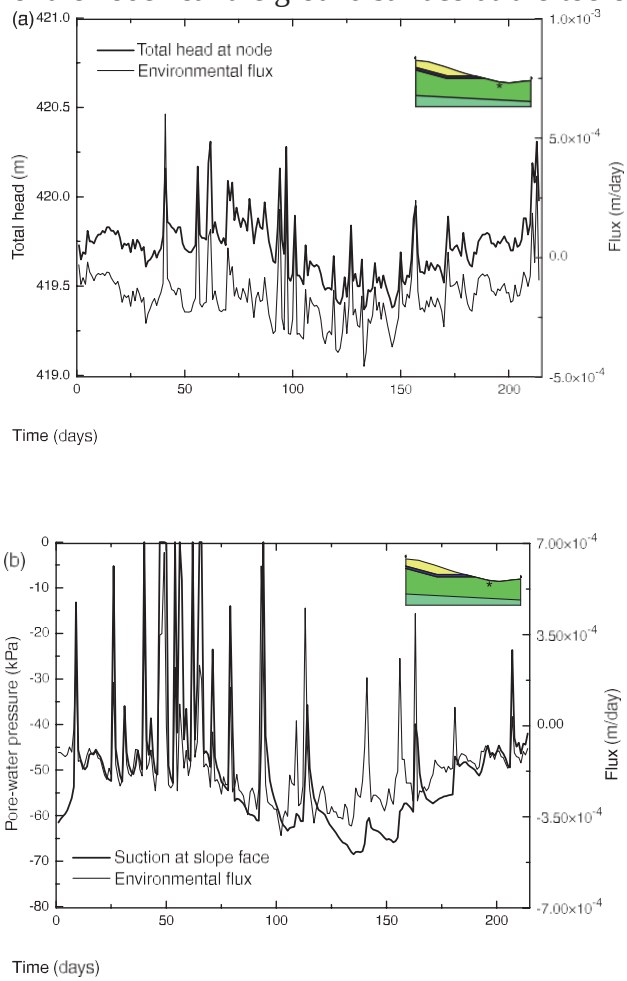

At this point, calibration of the seepage model was con- sidered acceptable, since both the groundwater and soil suctions were modeled reasonably well over the extended period of field measurements in 2000. Further improvements could no doubt be made to either the modeled groundwater

the environmental flux function with respect to time. The agreement is not quite as close as with the total head results in Fig. 14*a*, however. Deeper points in the profile than the shallow node in Fig. 14*b* showed larger time lags between a large positive flux event at the ground surface and the corre- sponding increase in total head.

Transient slope stability analysis

The modeled pore-water pressure distributions for 1999 and 2000 were imported into a limit equilibrium slope sta- bility application (Slope/W) to examine the variation of the factor of safety during the same period of time. The analysis used a fully specified failure surface based on observations in the test pits and boreholes (Fig. 15).

Table 2 shows the soil parameters used in the modeling. The friction angle for suction, ϕ^b, reflecting the changes in soil shear strength associated with changes in suction, was assumed to be equal to ϕ' (Vanapalli et al. 1996), the effec- tive angle of shearing resistance of a saturated soil,

ISSN: 2278-4632
Vol-10 Issue-1 January 2020

based on the fact that the suctions were near or at the AEV in the weathered and unweathered clay for the majority of the pe- riod being modeled. The soil parameters used for the silty fine sand seam were taken simply as typical values. The ef- fect of this assumption will be limited due to the location and small thickness of the sand seam (typically the sand seam only affected two slices in the slope analysis). The silty fine sand seam was assumed to be saturated, and no ψ^b was required.

Slope stability results

Upon completion of the transient seepage analyses for 1999 and 2000, the corresponding slope stability of the slope for the same periods was examined using the Morgenstern–Price method in Slope/W with a constant interslice force function. Figure 16 shows the variation of the factor of safety (FS) with time for the years 1999 and 2000. The calculated factors of safety remain significantly above 1.0 during 2000, with a minimum factor of safety of 1.72. Varia-tions in the factor of safety correspond to changes in the sea-sonal wetness but were relatively small, in the range 1.7–2.2. In contrast, the modeled factors of safety for 1999, the year the slope failed, exhibited considerable variation within

profile or the suction profile. However, the nature of the saturated–unsaturated flow regime restricts adjustments. As expected from the close linkage between storage and trans- mission of water in the soil, improving one aspect of the modeling, for example the groundwater profile, appeared to worsen the other aspect, in this case the soil suction profile.

Results of transient seepage analysis

Figure 14*a* plots total head and the environmental flux boundary function versus time for a node near the ground surface at the toe of the slope. There is good agreement be- tween the environmental flux function and the head profile. This level of agreement was broadly achieved throughout the profile.

In addition to directly affecting the pore-water pressure profile near the ground surface, the environmental flux boundary condition also influences the soil suction profile (Fig. 14*b*). As with the groundwater profile, there is gener- ally a strong correlation between the soil suction profile and short periods of only a few days. For the most part, signifi- cant fluctuations in the factor of safety occurred in May and June (days 30–60), corresponding to the extended periods of rainfall represented by the environmental flux boundary function in Fig. 11. Figure 16 shows several occasions dur- ing days 30–60 in 1999 when the calculated factors of safety were only marginally above unity (FS ≈ 1.04). These factors of safety suggest that slope movements could have occurred. The effect of long-duration, low-intensity events is reflected in decreases in the modeled factor of safety from higher val- ues (around 2.0) to values just above unity.

After about day 100, the factors of safety for 1999 and 2000 correspond closely with each other. Having similar fac- tors of safety after day 100 indicates there is a natural equi- librium for the slope related to average moisture conditions in the area. Based on the data from 1999, instability issues occurred in the months following spring thaw when exten- sive rainfall occurred. Stability returned during the dry heat of midsummer.

Fig. 15. Slope/W domain used in the stability analysis.

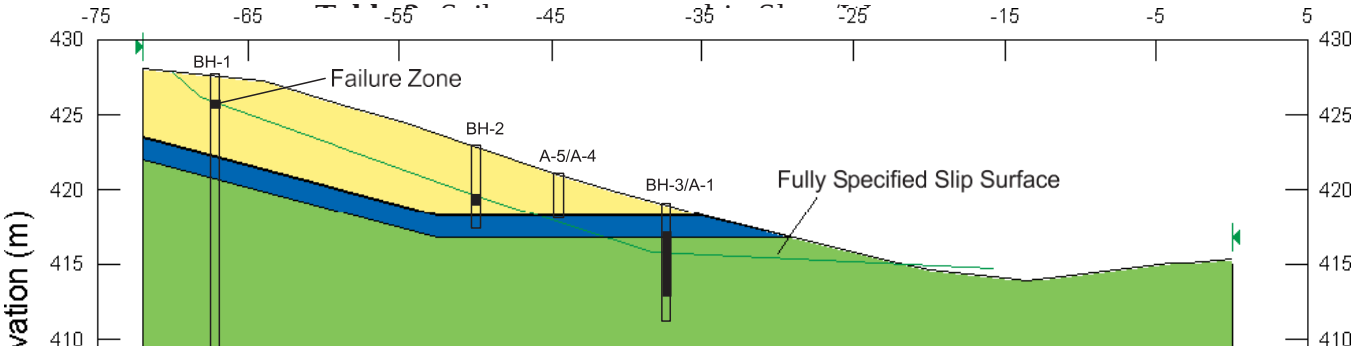

ISSN: 2278-4632
Vol-10 Issue-1 January 2020

ϕ_{nc} (°)	22	37
c	0	0
ϕ_b (°)	22	na
γ_{bulk} (kN/m^3)	19.6	19.6

Note: na, not available; γ_{bulk}, bulk density.

Fig. 17. Frictional and suction component of available shearstrength.

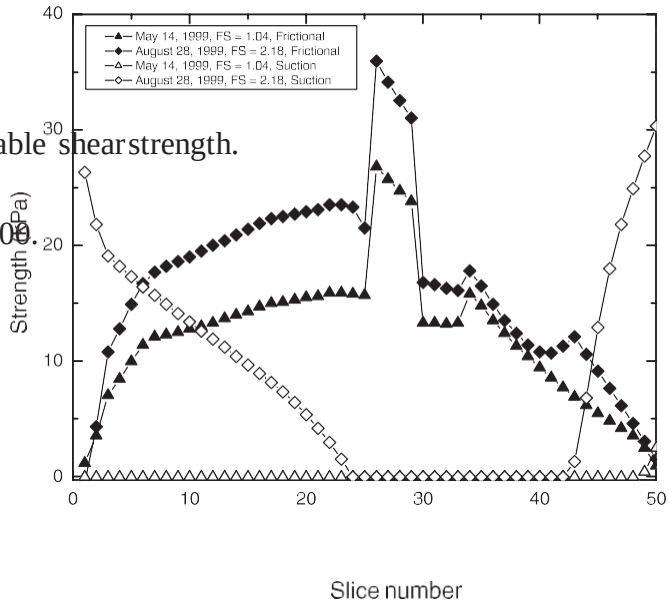

Fig. 16. Transient factor of safety for 1999 and 2000.

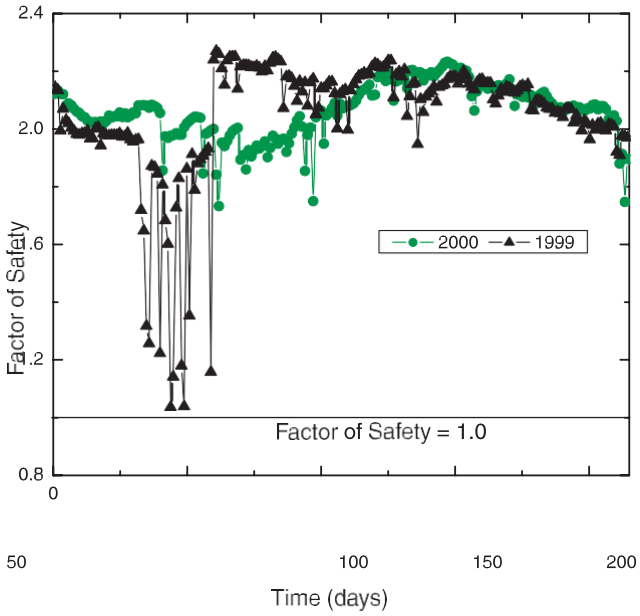

At this point, the modeling shows decreases in factor of safety corresponding to increases in infiltration rates associ- ated with measured rainfall. To understand the mechanisms involved, the pore-water pressures and forces on the failure surface should be examined.

Figure 17 shows results from two simulations, one unsta- ble (14 May 1999) and one stable (28 August 1999). Fig- ure 17 examines the available frictional and matric suction components of shear strength along the base of identical fail- ure surfaces. Slice 1 is located near the crest of the slope and slice 50 is near the toe. Figures 18*a* and 18*b* show corre- sponding pore-water pressure contours in the slope during the same 2 days. Because the groundwater pressures are higher on 14 May than on 28 August, there is less available frictional shear strength in the unstable slope. As well, there is no (or little) contribution to shear strength from the soil suction, since pore-water pressures are close to zero every- where due to influx of water from the ground surface. In contrast, the simulation for 28 August shows a substantial component of shear resistance provided by suction. Suction-

ISSN: 2278-4632
Vol-10 Issue-1 January 2020

Fig. 18. Pore-water pressure distribution: (*a*) 14 May 1999; (*b*) 28 August 1999. Pressure contours

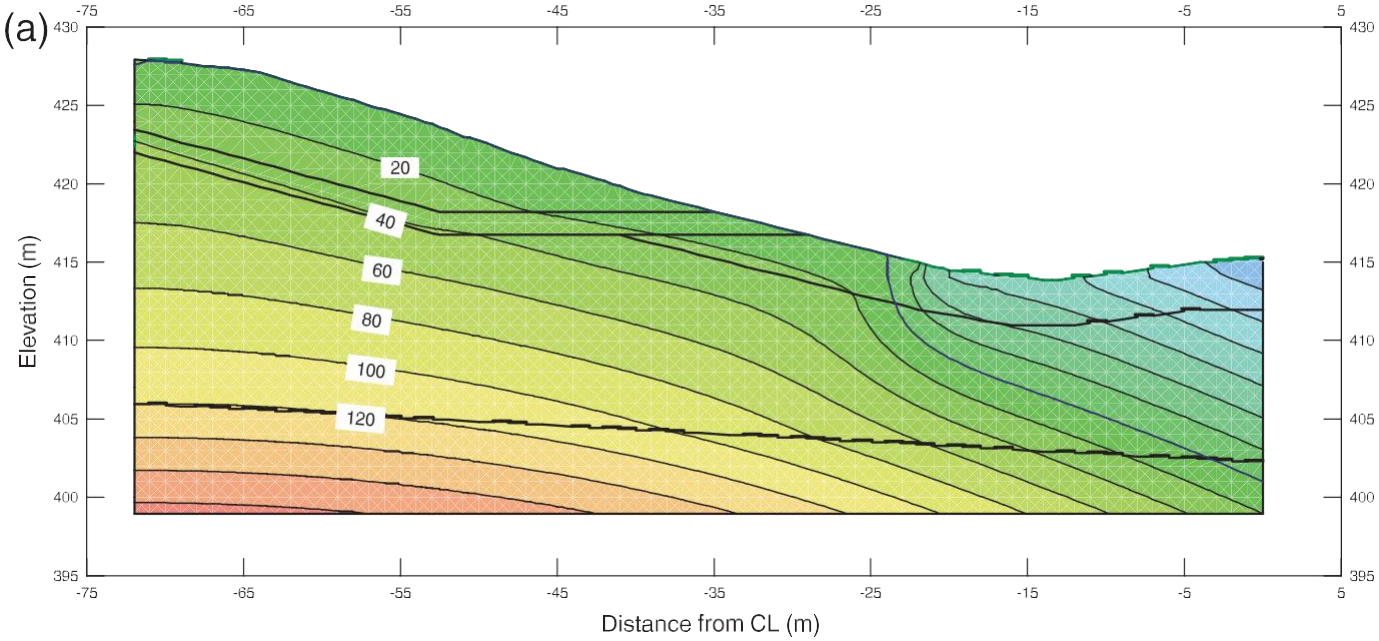

in kPa.

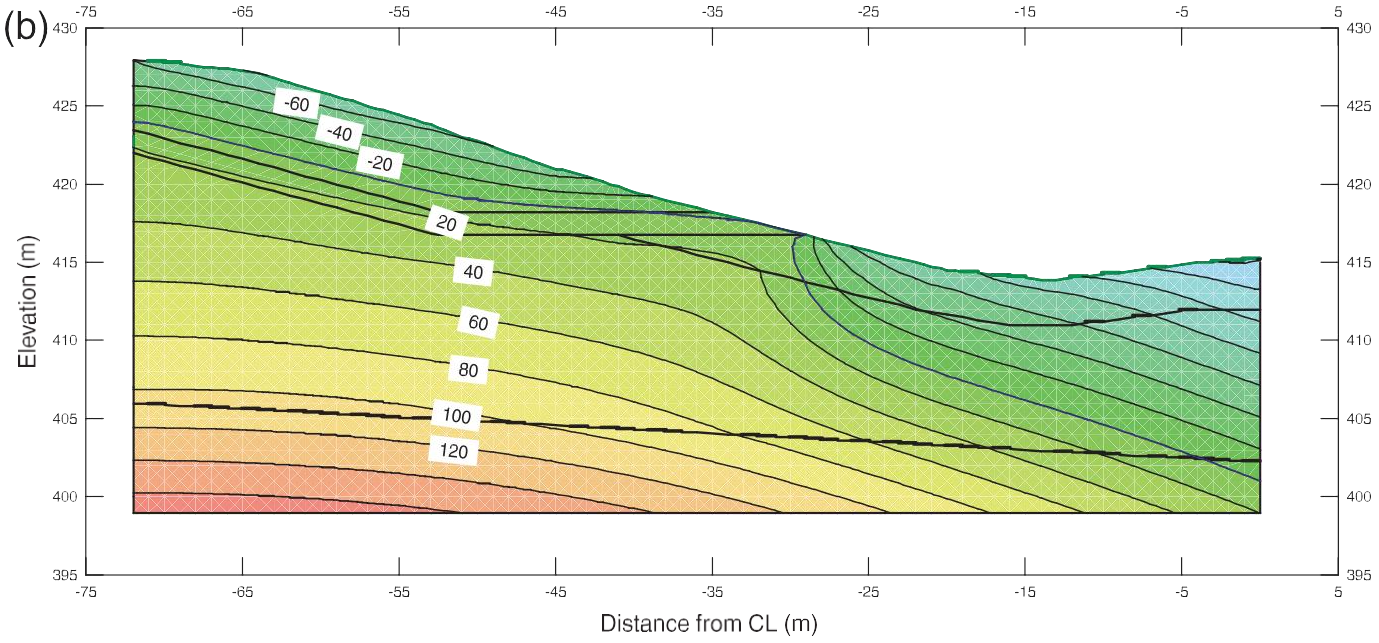

ISSN: 2278-4632
Vol-10 Issue-1 January 2020

dependent shear strength is the primary reason for the high factor of safety and the stable slope.
The transient groundwater flow model, which incorpo- rated the boundary flux as a function of the observed weather conditions, showed that during 1999 the soil suction dissipated as the groundwater level approached the surface. The subsequent limit equilibrium modeling showed that the loss of the soil suction brought the slope to an unstable con- dition.

Sensitivity analysis

Further analyses were performed to determine the sensi- tivity of the calculated factors of safety to adjusted,as-
sumed, or estimated values of evapotranspiration, recharge into the silty fine sand seam (the left side boundary), □□ forthe silty fine sand seam, and □□ for the unweathered claylayer. Figure 19 shows how the factor of safety changes with various selected values of these variables. The simulations were run for 14 May 1999 when the best estimate of the fac- tor of safety was 1.14. This allowed for a fairly significant reduction in the factor of safety before reaching unity. The factor of safety is relatively sensitive to changes in evapo- transpiration and changes in □□ for the unweathered clayey silt (Figs. 19*a* and 19*d*, respectively). The sensitivity of the model to changes in evapotranspiration was expected. Evapotranspiration directly impacts the magnitude of re-

1125

Fig. 19. Factor of safety versus (*a*) percent change in evapotranspiration, (*b*) change in head at the left boundary,
(c) internal friction angle (□) of the silty fine sand seam, and
(d) □ of the unweathered clayey silt.

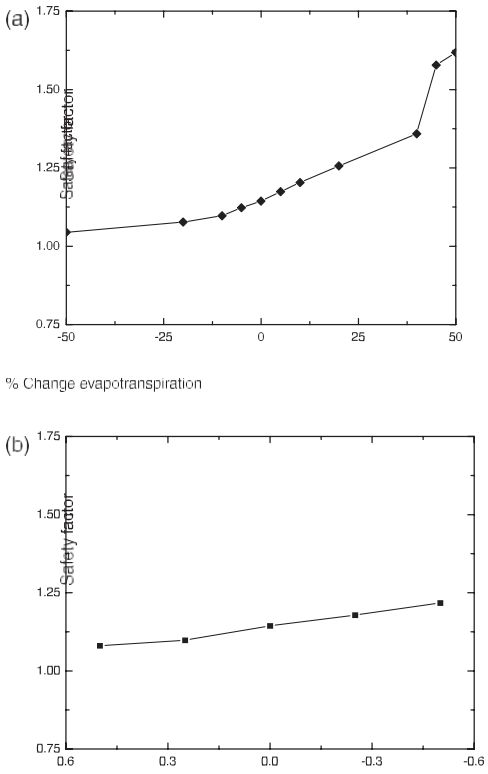

ISSN: 2278-4632
Vol-10 Issue-1 January 2020

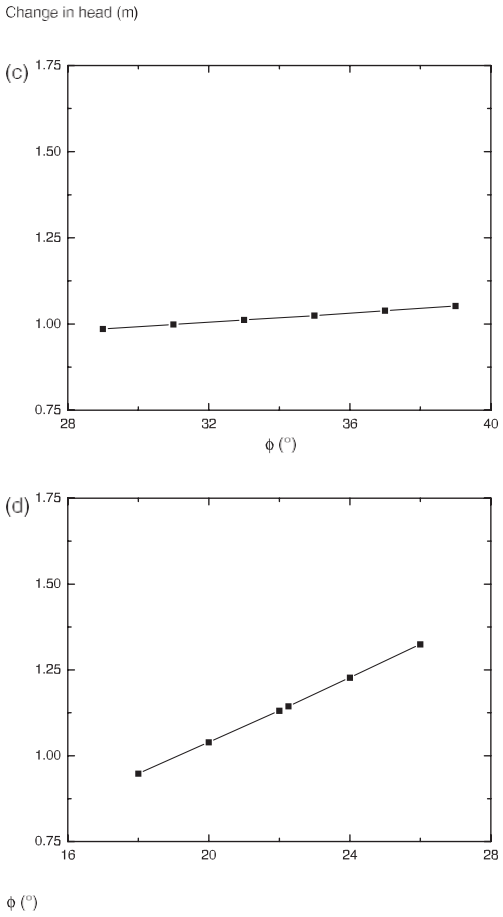

charge during a rainfall event and therefore the propensity of the infiltration to reduce the available shear strength through dissipation of the matric suction profile. The value of the evapotranspiration variable derived from the calibration for year 2000 was also used for the predictions for year 1999. Since calibration of the model for precipitation data fromyear 2000 showed good agreement for both the groundwater levels and suction profile, the value of evapotranspiration was considered reasonable. The sensitivity to changes in □□ for the unweathered clayey silt was not a concern because there was confidence that direct shear and triaxial testing had produced consistent results (Figs. 9*b*, 9*c*).

Apart from the significant effect of evapotranspiration, the sensitivity analysis demonstrated that the model parameters that had been assumed, adjusted, or estimated had only min- imal effects on calculated factors of safety. The sensitivity of the model to changes in evapotranspiration was considered acceptable based on model calibration using field measure- ments from a year (2000) different from the year in whichthe slope failed (1999). Additional work could be usefully directed in this application to improved methods of assign- ing the evapotranspiration parameter using better methodssuch as those developed by Wilson et al. (1994, 1997) andby experimental measurement of the unsaturated soil prop- erty functions using well-established laboratory testing methods.

Discussion and conclusions

Soil suction contributes significantly to the available shear strength in unsaturated soil materials. This study shows that soil suction can be a dominant component of strength in maintaining stable

ISSN: 2278-4632
Vol-10 Issue-1 January 2020

conditions in slopes, even in climates where unsaturated soil conditions have not previously re- ceived close attention. Infiltration of rainfall into a soil pro- file reduces the soil suction, thereby reducing available shear strength. The decreases of soil suction can be modeled using transient groundwater modeling with appropriate unsaturated soil property functions and proper definition of the flux boundary condition. Near-surface conditions are dominated by the environmental (weather) conditions that can be appro- priately modeled using known theories that incorporate time- dependent environmental parameters. Sensitivity analysis of the strength and flow boundary conditions in this work dem- onstrated that the most significant parameter for the determi- nation of this mode of instability was characterization of the environmental boundary conditions and, in turn, the changes in soil suction.

References

ASTM. 1990. Standard test method for measurement of hydraulic conductivity of saturated porous material using a flexible wall permeameter (D5084-90). *In* 1990 Annual Book of ASTM Stan- dards, Vol. 04.08. American Society for Testing and Materials (ASTM), Philadelphia, Pa. pp. 985–992.

ASTM. 1993. Standard test method for direct shear test of soils un- der consolidated drained conditions (D3080-90). *In* 1993 An- nual Book of ASTM Standards, Vol. 04.08. American Society for Testing and Materials (ASTM), Philadelphia, Pa. pp. 417– 422.

ASTM. 1995. Standard test method for consolidated undrained triaxial compression test for cohesive soils (D4767). *In* 1995 Annual Book of ASTM Standards, Vol. 04.08. American Soci- ety for Testing and Materials (ASTM), Philadelphia, Pa. pp. 882–891.

Aubertin, M., Ricard, J.-F., and Chapuis, R.P. 1998. A predictive model for the water retention curve: application to tailings from hard-rock mines. Canadian Geotechnical Journal, **35**: 55–69.

Baracos, A., and Graham, J. 1981. Landslide problems in Winni- peg. Canadian Geotechnical Journal, **18**: 390–401.

Betcher, R.N. 1983. Water resources, Virden area (62-F). Ground- water Availability Map Series, Manitoba Natural Resources, Winnipeg, Man.

Brand, E.W., Premchitt, J., and Phillipson, H.B. 1984. Relationship between rainfall and landslides in Hong Kong. *In* Proceedings of the 4th International Symposium on Landslides, Toronto, Ont., 16–21 September 1984. BiTech Publishers, Vancouver, B.C. Vol. 1, pp. 377–384.

Domaschuk, L. 1977. Soil block sampler. Canadian Geotechnical Journal, **14**: 262–265.

Ferreira, N.J. 2002. Assessing the effect of near surface environ- mental conditions on unsaturated slope instability. M.Sc. thesis, Department of Civil Engineering, University of Manitoba, Win- nipeg, Man.

Fredlund, D.G., and Rahardjo, H. 1993. Soil mechanics for unsatu- rated soils. Wiley Publications, New York.

Klassen, R.W. 1975. Quaternary geology and geomorphology of Assiniboine and Qu'Appelle valleys of Manitoba and Saskatche- wan. Geological Survey of Canada, Bulletin 228.

Klassen, R.W., and Wyder, J.E.1970. Bedrock topography, buried valleys and nature of drift, Virden map-area. Geological Surveyof Canada, Paper 70-56.

Kovács, G. 1981. Seepage hydraulics. Science Publishers, Amster- dam.

Krahn, J., Fredlund, D.G., and Klassen, M.J. 1989. Effect of soil suction on slope stability at Notch Hill. Canadian Geotechnical Journal, **26**: 269–278.

Lim, T.T., Rahardjo, H., Chang, M.F., and Fredlund, D.G. 1996. Effect of rainfall on matric suctions

ISSN: 2278-4632
Vol-10 Issue-1 January 2020

in a residual soil slope. Ca- nadian Geotechnical Journal, **33**: 618–628.

Meyer, A.F. 1944. Evaporation from lakes and reservoirs. Minne- sota Resources Commission, St. Paul, Minn.

Misfeldt, G.A., Sauer, E.K., and Christiansen, E.A. 1991. The Hep- burn landslide: an interactive slope-stability and seepage analy- sis. Canadian Geotechnical Journal, **28**: 556–573.

Penman, H.L. 1948. Natural evapotranspiration from open water, bare soils and grass. Proceedings of the Royal Society of Lon- don, Series A, **193**: 120–145.

Rivard, P.J., and Lu, Y. 1978. Shear strength of soft fissured clays. Canadian Geotechnical Journal, **15**: 382–390.

Shaw, R.J., and Hendry, M.J. 1998. Hydrogeology of a thick claytill and Cretaceous clay sequence, Saskatchewan, Canada. Cana- dian Geotechnical Journal, **35**: 1041–1052.

Tutkaluk, J., Graham, J., and Kenyon, R.M. 1998. Effects of river- bank hydrogeology on riverbank stability. *In* Proceedings of the 51st Canadian Geotechnical Conference, Edmonton, Alta., 4– 7 October 1998. Canadian Geotechnical Society, Alliston, Ont., Vol. 1, pp. 283–288.

Vanapalli, S.K., Fredlund, D.G., Pufahl, D.E., and Clifton, A.W. 1996. Model for the prediction of shear strength with respect to soil suction. Canadian Geotechnical Journal, **33**: 379–392.

van Genuchten, M.Th. 1980. A closed-form equation for predicting the hydraulic conductivity of unsaturated soils. Soil Science So- ciety of American Journal, **44**: 892–898.

Viklander, P. 1998. Permeability and volume changes in till due to cyclic freeze/thaw. Canadian Geotechnical Journal, **35**: 471– 477.

Wilson, G.W., Fredlund, D.G., and Barbour, S.L. 1994. Coupled soil–atmosphere modelling for soil evaporation. Canadian Geotechnical Journal, **31**: 151–161.

Wilson, G.W., Fredlund, D.G., and Barbour, S.L. 1997. The effect of soil suction on evaporative fluxes from soil surfaces. Cana- dian Geotechnical Journ al, **34**: 145–155.